Rapid Communication

Continuous non-invasive optical monitoring of cerebral blood flow and oxidative metabolism after acute brain injury

Wesley B Baker[1,2,]* ⓘ, Ramani Balu[3,]*, Lian He[4],
Venkaiah C Kavuri[4], David R Busch[4,5], Olivia Amendolia[6],
Francis Quattrone[6], Suzanne Frangos[6],
Eileen Maloney-Wilensky[6], Kenneth Abramson[4],
Elizabeth Mahanna Gabrielli[1] ⓘ, Arjun G Yodh[4] and
W Andrew Kofke[1]

Abstract

Rapid detection of ischemic conditions at the bedside can improve treatment of acute brain injury. In this observational study of 11 critically ill brain-injured adults, we employed a monitoring approach that interleaves time-resolved near-infrared spectroscopy (TR-NIRS) measurements of cerebral oxygen saturation and oxygen extraction fraction (OEF) with diffuse correlation spectroscopy (DCS) measurement of cerebral blood flow (CBF). Using this approach, we demonstrate the clinical promise of non-invasive, continuous optical monitoring of changes in CBF and cerebral metabolic rate of oxygen ($CMRO_2$). In addition, the optical CBF and $CMRO_2$ measures were compared to invasive brain tissue oxygen tension ($PbtO_2$), thermal diffusion flowmetry CBF, and cerebral microdialysis measures obtained concurrently. The optical CBF and $CMRO_2$ information successfully distinguished between ischemic, hypermetabolic, and hyperemic conditions that arose spontaneously during patient care. Moreover, CBF monitoring during pressor-induced changes of mean arterial blood pressure enabled assessment of cerebral autoregulation. In total, the findings suggest that this hybrid non-invasive neurometabolic optical monitor (NNOM) can facilitate clinical detection of adverse physiological changes in brain injured patients that are otherwise difficult to measure with conventional bedside monitoring techniques.

Introduction

After acute brain injuries, disruptions in cerebral autoregulation (CA) and metabolism can lead to secondary brain damage that markedly worsens outcome.[1–4] Accordingly, a key treatment strategy is to maintain cerebral blood flow (CBF) such that oxygen and glucose delivery match metabolic demands.[5–7] Reduced CBF relative to metabolic needs can induce secondary ischemic damage, whereas excess CBF can cause blood–brain barrier (BBB) disruption, edema formation, and hemorrhage. Ideally, bedside monitors will detect conditions that increase the likelihood of

[1]Department of Anesthesiology and Critical Care, University of Pennsylvania, Philadelphia, PA, USA
[2]Division of Neurology, Department of Pediatrics, Children's Hospital of Philadelphia, Philadelphia, PA, USA
[3]Department of Neurology, University of Pennsylvania, Philadelphia, PA, USA
[4]Department of Physics and Astronomy, University of Pennsylvania, Philadelphia, PA, USA
[5]Department of Anesthesiology & Pain Management and Neurology & Neurotherapeutics, University of Texas Southwestern, Dallas, TX, USA
[6]Department of Neurosurgery, University of Pennsylvania, Philadelphia, PA, USA

*These authors contributed equally to this work.

Corresponding author:
Wesley B Baker, 3231 Walnut Street, Philadelphia, PA 19104, USA.
Email: bakerw@email.chop.edu

secondary injury.[6–11] Unfortunately, however, bedside monitoring techniques (including serial neurologic examinations) in current use are unable to provide real-time, continuous, non-invasive measurements of CBF and brain metabolism.[6–9] This leads to a situation wherein mismatches between perfusion and metabolism that commonly arise in the hospital are often not detected until after irreversible brain damage has developed.

Invasive monitors placed directly into brain tissue can serially measure intracranial pressure (ICP), brain interstitial oxygen tension ($PbtO_2$), CBF, and tissue biochemistry (using cerebral microdialysis to serially measure lactate, pyruvate, glucose, glycerol and glutamate) at a single spatial location in the white matter. While these monitors can provide real-time information about the adequacy of cerebral perfusion, only a small fraction of patients with acute brain injury receive invasive probes. Furthermore, data from a single white matter location may not always be indicative of cortical tissue, and invasive monitors do not directly measure mismatches between perfusion and metabolism. Invasive ICP probes do permit calculation of cerebral perfusion pressure (CPP) from mean arterial pressure (MAP) and ICP measurements, i.e., as the difference between MAP and ICP, but quite often, population-based CPP targets[12–14] are not applicable for individual patients. Indeed, hypoxic/ischemic secondary damage can occur even when target CPP levels are maintained.[15–17] In principle, thermal diffusion flowmetry (TDF) provides absolute CBF measurements with high temporal resolution; however, decreased CBF may not indicate ischemia since CBF reductions could be secondary to decreased cerebral metabolism. Moreover, TDF measurements are local, prone to measurement drift, and are less accurate/reliable when the probe is close to large vessels or if brain temperature is elevated.[18,19] Comparable tradeoffs exist for brain tissue oxygen monitoring and microdialysis, since $PbtO_2$ measurements may not always reflect the balance between oxygen delivery and consumption,[20,21] and since cerebral lactate elevations may reflect both ischemic and non-ischemic alterations in brain metabolic pathways.[22–24] Combining different invasive monitoring modalities could provide a more nuanced picture of the balance between metabolic supply and demand. However, treatment targets based on multi-modality intracranial monitoring are not standardized, and measurement variability makes unambiguous identification of cerebral ischemia difficult in real-time.

For the majority of patients, in whom invasive neuromonitoring is not feasible, clinicians are forced to rely on global, non-neurologic indicators of the adequacy of systemic perfusion coupled with serial neurological examinations. Unfortunately, global targets, e.g., MAP, P_aCO_2, systemic oxygen saturation, and serum pH, may be within normal limits during periods of cerebral physiological distress, and the sensitivity of the neurologic exam can be significantly depressed by both the acute insult and sedative medications. Electroencephalography (EEG)[25,26] and transcranial Doppler (TCD)[27] can provide non-invasive proxies of CBF; however, EEG signals are markedly altered by sedation, and TCD measurements are operator dependent, not amenable to prolonged continuous monitoring, and do not discriminate to changes in regional microvascular blood flow. Thus, a pressing clinical need for direct non-invasive CBF/metabolic monitors exists.

To this end, we tested the ability of a custombuilt non-invasive neurometabolic optical monitor (NNOM) to continuously and concurrently measure cortical CBF, oxygenation, and cerebral metabolism in patients with severe acute brain injury. The NNOM combines time-resolved near-infrared spectroscopy[28,29] (TR-NIRS) to measure regional cerebral microvascular oxygen saturation (StO_2) with diffuse correlation spectroscopy[30–32] (DCS) to measure an index of cortical CBF (F_c). Changes in StO_2 (combined with arterial oxygen saturation, SaO_2) can be used to estimate changes in the cerebral oxygen extraction fraction (OEF),[33] and in combination with measurements of F_c, enable calculation of cerebral metabolic rate of oxygen ($CMRO_2$).[33–35] In this way, deleterious mismatches between perfusion and metabolism can be identified. The prolonged ICU bedside monitoring of CBF, OEF, and $CMRO_2$ demonstrated herein augments and complements a recent report of CBF monitoring with DCS alone in the ICU setting.[36]

Previously, we utilized area under the curve (AUC) receiver-operator characteristic analysis to assess the ability of the individual components of NNOM (i.e., either DCS or TR-NIRS) to detect brain hypoxia (i.e., $PbtO_2 < 19\,mmHg$) in a subset of the patients reported here.[37] We found that NNOM CBF could detect brain hypoxia with fairly good predictive power (AUC = 0.76), but that NNOM StO_2 could not (AUC = 0.46).[37] A recent investigation of frequency-domain NIRS StO_2 monitoring for detection of brain hypoxia also showed variable predictive ability and was not robust across patients.[38] Of course, as mentioned above, brain hypoxia is not always equivalent to brain ischemia. Thus, we evaluated the capabilities of NNOM for detection of ischemia based on CBF and $CMRO_2$ data in combination. We further compared NNOM CBF and $CMRO_2$ to concurrent invasive $PbtO_2$, ICP, TDF, and cerebral microdialysis measurements obtained during standard clinical care,[6,11,39] and we used NNOM to assess CA state.

Methods

Patient selection and clinical monitoring

Written consent for all subjects was provided by legally authorized representatives, and all protocols/procedures were approved by the institutional review board at the University of Pennsylvania, which adheres to the guidelines of the Common Rule and the Food and Drug Administration's Institutional Review Board and human subject regulations. Adult patients admitted to the University of Pennsylvania Neurocritical Care Unit (NCCU) with severe traumatic brain injury (TBI), intracerebral hemorrhage (ICH), subarachnoid hemorrhage, or diffuse hypoxic–ischemic brain injury (HIBI) requiring invasive multi-modality neuromonitoring for clinical care were eligible for this observational study. Five TBI patients, three ICH patients, and three HIBI patients were enrolled ($N = 11$ total). The standard neuromonitoring bundle included placement of an ICP monitor (Camino, Natus Neuro, Middleton, WI), a Clark electrode (Licox, Integra LifeSciences, Plainsboro, NJ), a thermodilution CBF monitor (Bowman Perfusion Monitor, Hemedex, Cambridge, MA), and a cerebral microdialysis catheter (MDialysis, North Chelmsford, MA). Microdialysis allows for serial measurements of analytes that can diffuse from brain interstitial fluid across a dialysis membrane into artificial cerebrospinal fluid flowing continuously through the dialysis chamber. Hourly levels of cerebral lactate, pyruvate, glucose, glutamate, and glycerol are routinely measured for clinical care.

Elevated lactate and lactate:pyruvate ratio (LPR) are both markers of anaerobic ischemia, while reduced cerebral glucose is a marker of metabolic distress from either excess consumption or reduced delivery.[40–42] Glutamate and glycerol are markers of excitotoxicity and cell membrane turnover, respectively. Invasive probes were inserted through a quad lumen bolt (Hemedex, Cambridge, MA) placed above Kocher's point[11] (Figure 1(a), (c)). Data from the invasive monitors, as well as other physiological variables (e.g., MAP, end-tidal CO_2), were continuously recorded and time-synchronized using a bedside recording unit (CNS Monitor, Moberg Research Inc, Ambler, PA).[11]

Radiographic scores of injury severity (Marshall Grade for TBI,[43] ICH score for ICH[44]) were calculated from initial CT scans of TBI and ICH patients enrolled in the study. Events of interest that naturally arose during the course of standard clinical care ($n = 120$) were annotated by bedside nurses or clinical research staff on the CNS monitor during optical monitoring, and then retrospectively reviewed to identify episodes for further analysis. Events were divided into the following categories: (1) patient agitation ($n = 6$); (2) clinical examination ($n = 3$); (3) nursing manipulations, including bathing ($n = 1$), oral care ($n = 11$), bed position changes ($n = 17$), and suctioning ($n = 47$); (4) medications, including changes in vasoactive infusions ($n = 19$), administration of vasoactive boluses ($n = 3$), changes in sedative infusions ($n = 1$), and administration of hyperosmolar boluses ($n = 3$); (5) clinical procedures, including portable head CT
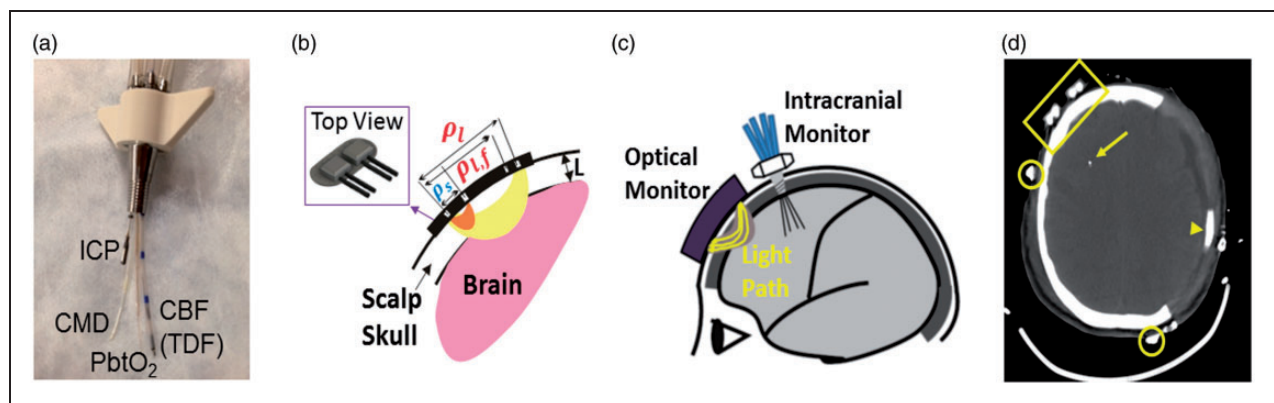

Figure 1. (a) Picture of quad lumen bolt with invasive probes. (b) Schematic of NNOM sensor that probes the head with: (1) TR-NIRS measurements at long ($\rho_l = 3.2$ cm) and short ($\rho_s = 0.7$ cm) source-detector separations to derive cerebral StO_2 and OEF; and (2) DCS measurements at long ($\rho_{l,f} = 2.5$ cm) and short ($\rho_s = 0.7$ cm) source-detector separations to derive a CBF index (see text). (c) Configuration of concurrent non-invasive and invasive intracranial monitoring probes. (d) Anatomical CT scan showing position of NNOM sensor on the scalp (encompassed by yellow rectangle) and the tip of an invasive probe (yellow arrow). The patient's skull was surgically removed from the left side to treat cerebral edema and intracranial hypertension. Arrowhead points to subdural drain, and open circles mark positions of EEG electrodes.

Table 1. Summary of clinical events.

ID	Agitation	Clinical exam	Nursing care	Meds	Clinical proc.	Storming	Events marked for further analysis
1			4				
2	1		5	2	1		Vasoactive medication change (1 event; Figure 5)
3			3	3			ICP crisis with mannitol administration (1 event; Figure 3)
4	1		5	9			Vasoactive medication changes (9 events; Figure 5)
5			3	3			Vasoactive medication changes (2 events; Figures 4 and 5)
6	1		5	1		1	Vasoactive medication change (1 event; Figure 5)
7			8		1	3	Autonomic storming event (1 event; Figure 2)
8			16	2	2		
9		3	19	5	1		Vasoactive medication changes (5 events; Figure 5)
10	1		4	1			Agitation & vasoactive medication change (2 events; Figures 2 and 5)
11	2		4				

Data are number of instances of the noted event.

($n = 1$), central line placement ($n = 1$), bronchoscopy ($n = 1$), nasogastric tube insertion ($n = 1$), and ventriculostomy tubing flush ($n = 1$); (6) autonomic storming events ($n = 4$, defined as abrupt increases in heart rate and blood pressure without other identifiable triggers). A summary of annotated events by subject, along with events marked for further study, is provided in Table 1.

NNOM monitoring

The custom-built NNOM instrument consisted of a TR-NIRS module and a DCS module to enable interleaved measurements of StO_2 and CBF index (F_c). The instrument and fiberoptic sensor are described in detail elsewhere.[45] Briefly, the NNOM sensor was placed on the forehead (Figure 1(b)), and secured with sweat-resistant double-sided tape (#1522 in contact with skin, #9917 in contact with sensor, 3 M Health Care, St. Paul, MN) reinforced with medical tape (Medipore Dress-It, #2954, 3 M) along the top edges. A black cloth spanning ~2–3 cm from the sensor edges was further employed to block stray room light. During patient monitoring, NNOM cyclically interleaved TR-NIRS measurements of temporal point spread functions at short (0.7 cm) and long (3.2 cm) separations at six wavelengths (730, 770, 786, 810, 830, 850 nm; 800 ms exposure per wavelength) with DCS measurements of normalized intensity autocorrelation functions (10 s exposure, short separation 0.7 cm, long separation 2.5 cm) to derive StO_2 and F_c every 20 s. From these data, indices of OEF and $CMRO_2$ were computed.

TR-NIRS analysis for cerebral OEF changes

For each TR-NIRS wavelength, we utilized a two-layer model of the head to estimate differential changes in cerebral tissue absorption; this analysis utilized the moments of the TR-NIRS temporal point spread functions measured at short and long separations (for details see Appendix in Supplementary material). Note, this analysis, which is a variation of a method described elsewhere,[46,47] assumes constant tissue reduced scattering to compute differential tissue absorption changes. The extra-cerebral layer thickness, *L*, was estimated for each patient from anatomical CT scans (e.g., Figure 1(d)). Concurrent tissue absorption measurements at the six TR-NIRS wavelengths were readily converted to concentration changes in cerebral oxy-hemoglobin (HbO) and deoxy-hemoglobin (Hb) via standard linear absorption spectroscopy theory.[48] The cerebral tissue oxygen saturation (StO_2) at any time is given by

$$StO_2 = \frac{HbO_o + \Delta HbO}{HbO_o + \Delta HbO + Hb_o + \Delta Hb} \quad (1) \leftarrow$$

where HbO_o and Hb_o are the baseline absolute oxy-hemoglobin and deoxy-hemoglobin concentrations, and ΔHb and ΔHbO are the respective changes in oxy- and deoxy-hemoglobin over time. HbO_o and Hb_o were obtained from multispectral estimates of cerebral tissue absorption gleaned from a nonlinear fit of the temporal point-spread function to the convolution of the impulse response function with the semi-infinite Green's function solution of the photon diffusion equation.[49,50] Relative changes in OEF were

then estimated from measurements of StO_2[33]

$$rOEF \quad \frac{OEF}{OEF_o} = \frac{SaO_2 \quad StO_2}{SaO_{2,o} \quad StO_{2,o}} \quad \frac{{}_o SaO_{2,o}}{SaO_2} \quad (2)\leftarrow$$

Here, SaO_2 is the arterial oxygen saturation obtained from a clinical pulse oximeter, and is a vascular partition weighting constant defined by the relation $StO_2 = (1 \quad)SaO_2 + \leftarrow SvO_2$. SvO_2 is the cerebral venous oxygen saturation. Note, throughout the manuscript, the subscript "o" indicates the baseline values. We assumed that $_o = \leftarrow$ in equation (2), which is valid if the distribution of cerebral blood volume across the arterial, capillary, and venous compartments is similar for the baseline and "perturbed" time points.

DCS analysis for CBF changes

Utilizing a previously described probe pressure measurement paradigm,[51] we employed a two-layer model of the head to derive a CBF index (F_c) from the temporal autocorrelation functions measured at short and long separations. Constant tissue reduced scattering was assumed for this computation, and the TR-NIRS-derived tissue absorption measurements (at the 786 nm wavelength) were used as inputs in the pressure measurement paradigm for computing F_c. Changes in CBF relative to baseline were estimated from changes in F_c.[52,53]

$$rCBF \quad CBF/CBF_o = F_c/F_{c,o} \quad (3)\leftarrow$$

TR-NIRS/DCS measurement of CMRO$_2$

We used a steady-state tissue compartment model to estimate changes in the $CMRO_2$ from TR-NIRS and DCS measurement of OEF and CBF changes, respectively[33,54]

$$rCMRO_2 \quad CMRO_2/CMRO_{2,o}$$
$$= (OEF/OEF_o) \quad (CBF/CBF_o)\leftarrow \quad (4)\leftarrow$$

where OEF/OEF_o and CBF/CBF_o are given by equations (2) and (3). Equation (4) is valid for comparing $CMRO_2$ between different tissue states that experience steady-state conditions,[54] i.e. the cerebral oxygen concentration in the blood, oxygen concentration in the tissue, and blood volume are assumed constant (but different) in the baseline (i.e., denoted by subscript "o") and "perturbed" states. Equation (4) further assumes that arterial oxygen concentration in the blood does not change.

Assessment of CA from NNOM measurements

Correlation-based autoregulation indices were calculated from 19 different time-periods where MAP varied by >10 mmHg in response to changes in vasoactive medication infusion rates. We calculated Pearson's correlation coefficient (DCSx) between the NNOM F_c index and MAP across the temporal interval spanning from 10 min prior to 40 min after the infusion rate adjustment. Note, to prevent the same data from being used for multiple CA assessments in cases where multiple infusion rate adjustments were administered less than an hour apart, only the first adjustment in the series was considered. The pressure reactivity index (PRx; Pearson's correlation coefficient between ICP and MAP),[55] brain tissue oxygen pressure reactivity index (ORx; Pearson's correlation between $PbtO_2$ and CPP),[56] cerebral oximetry index (COx; Pearson's correlation between StO_2 and MAP),[57] and TDF CBF index (TDFx; Pearson's correlation between TDF CBF and CPP) were also computed across the same temporal intervals. Positive values for these correlation indices indicate impaired autoregulation, whereas a lack of correlation indicates preserved autoregulation. Note, negative PRx values also suggest intact CA, since vasoconstriction triggered by MAP increases will decrease cerebral blood volume, which ultimately causes a decrease in ICP. The COx, which is computed from NNOM StO_2 data, employs StO_2 changes as a surrogate for CBF changes.[57]

Results

Eleven adult patients admitted to the University of Pennsylvania NCCU with either severe TBI ($N=5$), ICH ($N=3$), or diffuse HIBI ($N=3$) were enrolled in this observational study. All patients had a bundle of invasive monitors placed into frontal lobe white matter to guide clinical care. The standard bundle consisted of invasive ICP, $PbtO_2$, CBF, and cerebral microdialysis monitors inserted through a multi-lumen bolt (Figure 1). Optical monitoring was performed during routine clinical care for a median of 7 h/day per patient (range 1.5–8.5 h/day) and was compared directly with data obtained from the invasive monitors. Patients were monitored for a median duration of three days (range 1–4 days). Across all patients, 207 h of NNOM data were collected and the median length of optical monitoring per patient was 17.5 h (range 6.5–31.5 h). A summary of the clinical patient characteristics and monitoring details for the studied cohort is provided in Table 2.

Correlation between absolute invasive and non-invasive measurements

We initially compared the absolute properties determined by invasive and non-invasive methods using all

Table 2. Patient clinical and study data.

ID	Age (Sex)	Injury mechanism, details	Out-come	NNOM start (post injury day)	Days (total hours) monitored	Concurrent invasive monitors	Invasive monitor location	NNOM probe location
1	29 (M)	TBI, Motorcycle crash Marshall grade II	Rehab	2	3 (15)	ICP, PbtO$_2$, TDF	Left frontal	Right frontal
2	63 (F)	ICH, R BASAL Ganglia ICH score 2	Nursing home	2	2 (6.5)	ICP, PbtO$_2$, TDF, CMD	Left frontal	Left frontal
3	38 (F)	HIBI, Opiate overdose PEA arrest	Nursing home	4	1 (7)	ICP, PbtO$_2$, TDF	Right frontal	Right frontal
4	33 (M)	HIBI, GSW to neck PEA arrest	Died	2	4 (29)	ICP, PbtO$_2$, TDF	Right frontal	Right frontal
5	33 (M)	TBI, GSW to head Marshall grade V/VI	Rehab	4	4 (27)	ICP, PbtO$_2$, TDF	Left frontal	Right frontal
6	26 (M)	TBI, Motorcycle crash Marshall grade II	Rehab	10	2 (12.5)	ICP, PbtO$_2$	Left frontal	Right frontal
7	47 (M)	HIBI, Cardiac arrest, rhythm unknown	Died	8	3 (17.5)	ICP, PbtO$_2$, TDF, CMD	Left frontal	Right frontal
8	57 (M)	ICH, R midbrain, IVH ICH score 3	Nursing home	4	3 (21)	ICP, PbtO$_2$, TDF, CMD	Left frontal	Left frontal
9	49 (F)	TBI, Fall down steps Marshall grade IV	Rehab	3	4 (31.5)	ICP, PbtO$_2$, TDF, CMD	Right frontal	Right frontal
10	62 (M)	ICH, R Basal ganglia ICH score 3	Nursing home	5	4 (27)	ICP, PbtO$_2$, TDF, CMD	Left frontal	Left frontal
11	27 (M)	TBI, Motorcycle crash Marshall grade III	Rehab	5	2 (12.5)	ICP, PbtO$_2$, CMD	Right frontal	Right frontal

TBI: traumatic brain injury; ICH: intracerebral hemorrhage; HIBI: diffuse hypoxic ischemic brain injury; GSW: gunshot wound; PEA: pulse electrical activity (cardiac arrest); NNOM: non-invasive neurometabolic optical monitor; ICP: intracranial pressure; PbtO$_2$: brain interstitial oxygen tension; TDF: thermal diffusion flowmetry; CMD: cerebral microdialysis.

patient data wherein TDF/DCS and PbtO$_2$/StO$_2$/DCS results were obtained concurrently. The absolute cortical CBF index (i.e., F_c) measured optically with DCS exhibited an overall poor correlation with absolute CBF measured with invasive TDF. Specifically, across the nine patients who had invasive blood flow monitoring, the mean Pearson correlation coefficient between invasive and optical CBF measurements was 0.15 (range: 0.35 to 0.60). There was a similar poor overall correlation between F_c and PbtO$_2$ (mean 0.25; range: 0.29 to 0.73), as well as between StO$_2$ and PbtO$_2$ (mean 0.25; range: 0.49 to 0.67), across all 11 patients. Despite the poor overall correspondence between the absolute optical and the absolute invasive measurements of CBF and oxygenation, however, we found that physiologically concordant changes between optically measured CBF, StO$_2$ and invasive monitors could clearly be identified during many of the clinical events of interest that were annotated during data collection (see Table 1). This set of events includes deleterious mismatches between cerebral perfusion and metabolism, and impaired CA.

Identification of metabolic supply/demand mismatches

In addition to providing information on CBF fluctuations, NNOM identified mismatches between cerebral metabolic demand and supply. By simultaneously monitoring CBF and StO_2, we were able to calculate the changes in OEF and $CMRO_2$ over time using a modified form of the Fick equation (equations (2) and (4)). Tracking these parameters permitted unambiguous identification of ischemia/misery perfusion episodes (defined by increased OEF and excess $CMRO_2$ compared to CBF) and hyperemia/luxury perfusion (defined by decreased OEF and excess CBF relative to $CMRO_2$). Ischemic episodes could further be categorized as being caused primarily by reductions in CBF (i.e., inadequate cerebral perfusion) or by elevations in $CMRO_2$ (i.e., excess cerebral metabolic demand). The following sections describe the examples of supply/demand mismatch in detail.

Ischemia from inadequate cerebral perfusion

During the course of care for an ICH patient undergoing NNOM monitoring (Subject 10), patient agitation triggered an abrupt increase in MAP from 98 to 120 mmHg (Figure 2(a)). In this setting, the phenylephrine infusion rate was rapidly titrated down to limit the risk of hematoma expansion. During the agitation event, there was a five-fold increase in $CMRO_2$ that was matched by an equivalent five-fold increase in CBF (Figure 2(b)). In addition, end-tidal CO_2 increased from 32 to 38 mmHg and invasive brain temperature slightly increased from 38.7 C to 39.2 C, consistent with abrupt increases in cerebral metabolism and perfusion, respectively. During the ensuing decrease in phenylephrine infusion rate (from 150 to 100 mcg/min), MAP decreased to 80 mmHg.

Although this blood pressure was within appropriate population-based goals for clinical care, NNOM and TDF measurements of CBF plummeted transiently to nearly zero, $PbtO_2$ dropped from 20 to 10 mmHg, and OEF increased two-fold (Figure 2(a)). After ~13 min, NNOM measurements of cortical CBF recovered, but OEF remained elevated, indicating an uncoupling between CBF and $CMRO_2$. CBF was depressed relative to $CMRO_2$ for the next 3.5 h (Figure 2(b)). The sustained mismatch between $CMRO_2$ and CBF triggered delayed increases in cerebral tissue LPR and glycerol measured using microdialysis, suggesting anaerobic metabolism and lipid membrane turnover from cell death, respectively (Figure 2(c)).[22,58,59] Recall, computation of $CMRO_2$ via equation (4) is valid for tissue states experiencing steady state conditions, which is not the case when cerebral oxygen concentration in

the blood and tissue experience rapid transient changes (see "Methods" section). Accordingly, we computed 6-min average $CMRO_2$ changes over hemodynamically stable intervals, rather than for every time point where F_c and OEF values were obtained.

Relative ischemia from excess cerebral metabolic demand

Figure 2(d) shows monitoring trends during an episode of paroxysmal sympathetic hyperactivity (PSH) in a patient with HIBI (subject 7). The event is marked by an abrupt increase in MAP and HR; note, no evidence of seizure activity was found in concurrent EEG monitoring. NNOM CBF increased abruptly during the event; however, the increase in $CMRO_2$ far exceeded the CBF change (reflected by a doubling of OEF, Figure 2(e)). The hypermetabolic-driven mismatch between $CMRO_2$ and CBF was accompanied by subtle increases in LPR and glycerol (Figure 2(f)), suggesting increased rates of anaerobic metabolism and cellular membrane turnover despite an overall increase in $PbtO_2$ during the PSH event (Figure 2(d)). The $CMRO_2$ increase likely reflects excess activity in hypothalamic and subcortical brain areas that mediate autonomic nervous system output to the periphery.

Cerebral hyperemia/luxury perfusion

Figure 3 shows an episode of intracranial hypertension in a patient with HIBI (subject 3) treated with mannitol. During the ICP spike, both MAP and ICP increased by ~20 mmHg, such that CPP remained relatively constant, and cortical CBF and $CMRO_2$ both decreased by ~25%. The matched reduction in CBF and $CMRO_2$ may reflect metabolic coupling to changes in CBF. Indeed, OEF and $PbtO_2$ remained relatively constant, suggesting that this episode of intracranial hypertension did not produce ischemic conditions. After mannitol administration, ICP decreased, but MAP remained relatively constant, resulting in a marked increase in CPP, a sustained increase in CBF relative to $CMRO_2$, and a decrease in OEF. This hyperemic mismatch between CBF and $CMRO_2$ was associated with an abrupt increase in $PbtO_2$.

CA assessment

For CA, we analyzed 19 instances across six patients (4 with TBI, 2 with ICH) in whom MAP changed by > 10 mmHg as a result of adjusting the infusion rates of vasoactive medications (nicardipine, $n = 4$; norepinephrine, $n = 14$; phenylephrine, $n = 1$). CA was characterized by the Pearson's correlation (DCSx) between concurrent NNOM CBF and MAP data across the
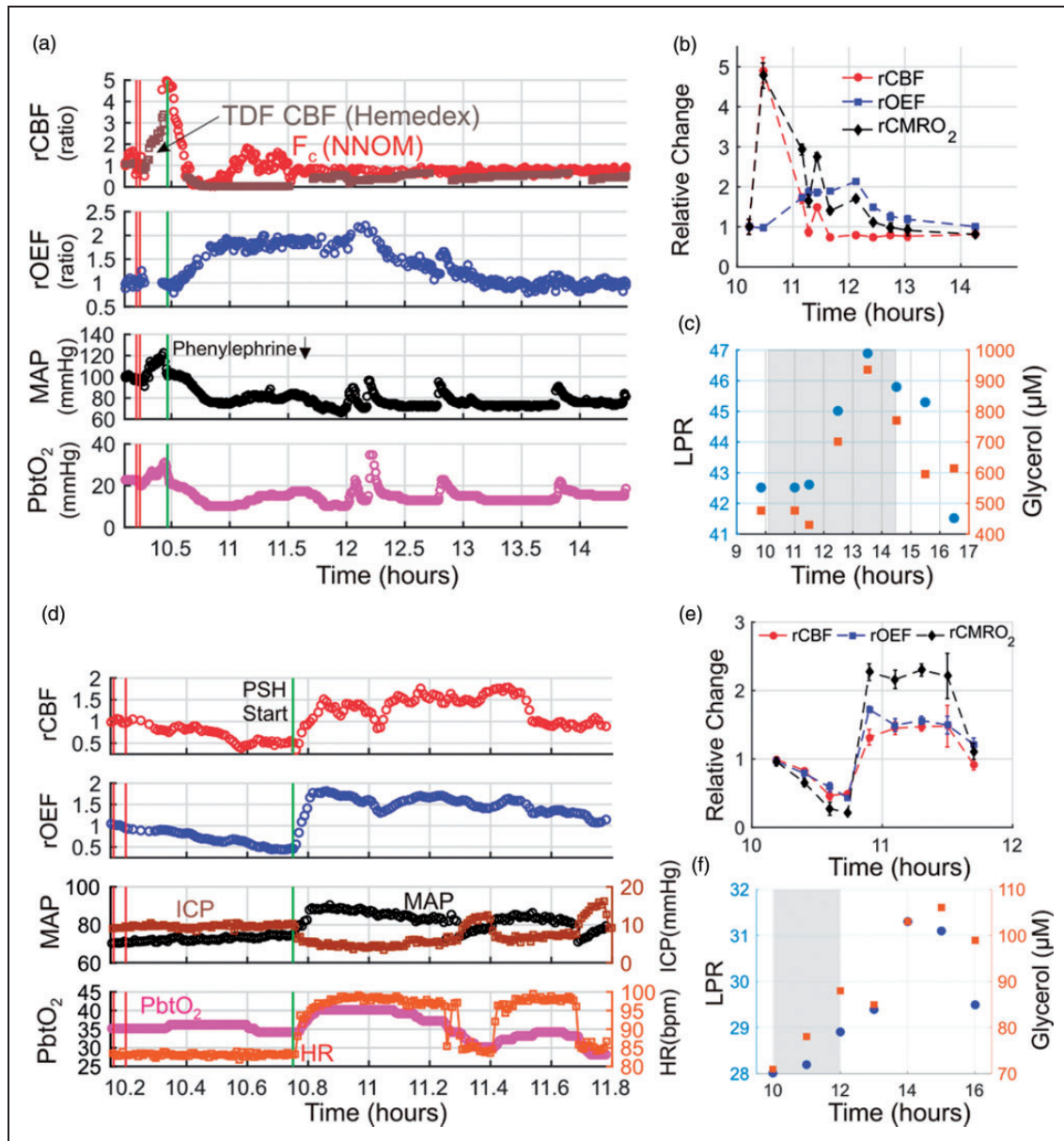
Figure 2. Cerebral ischemic events triggered by a decrease in mean arterial pressure (MAP) in subject 10 (a, b, c), and excess cerebral metabolic demand during paroxysmal sympathetic hyperactivity (PSH) in subject 7 (d, e, f). Temporal traces of multimodal data acquired before/during/after an episode of patient agitation (a) and before/during/after an episode of PSH (d). Relative cerebral oxygen extraction fraction (rOEF   OEF/OEF$_o$) and blood flow (rCBF   CBF/CBF$_o$) measurements obtained with the NNOM are given by equations (2) and (3), respectively. Baseline values, CBF$_o$ and OEF$_o$, are computed to be the means of the data between the two vertical red lines. Panel (a) contains NNOM measurements of cortical CBF (red circles) and thermal diffusion flowmetry (TDF) measurements of white matter CBF (brown squares). The vertical green lines in panels (a) and (d) indicate a decrease in phenylephrine infusion rate (from 150 to 100 mcg/min) and the start of PSH, respectively. In panels (b) and (e), steady-state 6-min averages of NNOM rCBF, rOEF, and relative cerebral metabolic rate of oxygen (rCMRO$_2$) data for the same temporal intervals as panels (a) and (d), respectively, are shown (rCMRO$_2$ given by equation (4)). Cerebral microdialysis lactate:pyruvate ratio (LPR; blue circles) and glycerol concentration (red squares) measurements are plotted before/during/after the patient agitation episode (c) and the PSH episode (f) over wider time intervals. The gray-shaded regions in panels (c) and (f) indicate the time intervals of panels (a) and (d), respectively. PbtO$_2$, ICP, and HR denote, respectively, brain interstitial oxygen tension, intracranial pressure, and heart rate. Note, the gap in NNOM data in panel (a) was caused by a regrettable crash in the instrument control software.
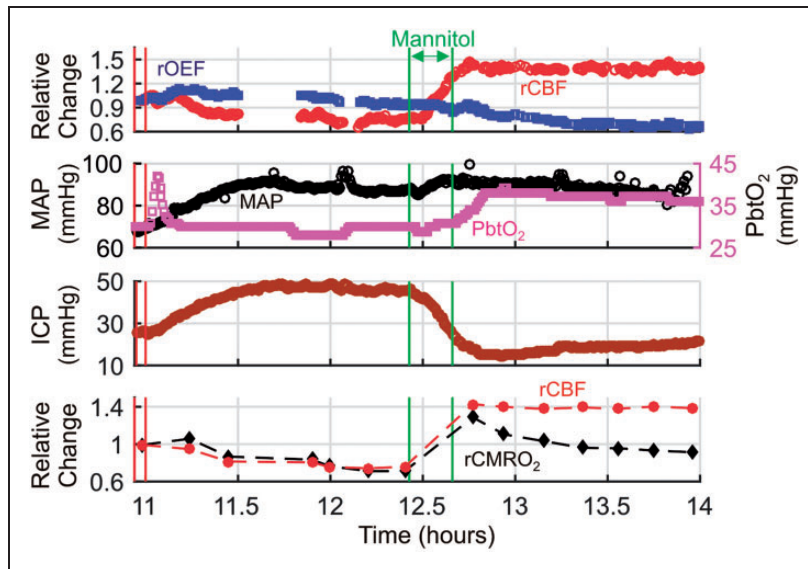
Figure 3. Hyperemia/Luxury perfusion after an episode of intracranial hypertension. Temporal traces of relative cerebral blood flow (rCBF $\equiv$ CBF/CBF$_o$), and oxygen extraction fraction (rOEF $\equiv$ OEF/OEF$_o$), mean arterial pressure (MAP), brain interstitial oxygen tension (PbtO$_2$), and intracranial pressure (ICP) data acquired during an episode of elevated ICP in a patient with diffuse hypoxic ischemic brain injury (cerebral microdialysis and thermal diffusion flowmetry CBF not available). Steady-state 6-min averages of rCBF and relative cerebral metabolic rate of oxygen (rCMRO$_2$ $\equiv$ CMRO$_2$/CMRO$_{2,o}$) data measured with the NNOM are also plotted versus time (bottom panel). CBF$_o$, OEF$_o$, and CMRO$_{2,o}$ denote the (baseline) mean values of the NNOM data between the two vertical red lines. The intracranial hypertension was treated with a 70 g bolus of 25% mannitol, administered between the two vertical green lines. Note: the initial transient increase in PbtO$_2$ at the beginning of the episode is due to a 100% O$_2$ challenge (performed periodically to test monitor function), and the gaps in the NNOM data were caused by regrettable crashes in the instrument control software.

temporal interval spanning from 10-min-prior to 40-min-after the infusion rate adjustment. TDF data were available for nine of the 19 identified "MAP challenges", and PbtO$_2$ data were available for 15 of the 19 challenges.

Two exemplar measurements of DCSx made in the same subject (subject 5) one day apart are shown in Figure 4. Interestingly, the first assessment in this subject indicated impaired CA (DCSx $= 0.92$, $p < 0.0001$; Figure 4(c)), but the second assessment performed 26.3 h later indicated intact CA (DCSx $= -0.07$, $p = 0.5$; Figure 4(d)). The shift from high to low DCSx values suggests a progressive improvement in CA over time. Indeed, the patient ultimately had a return of consciousness and was discharged to an acute rehabilitation facility.

As discussed above, other indices of CA include the ORx (correlation between PbtO$_2$ and CPP), TDFx (correlation between TDF CBF and CPP), COx (correlation between NNOM StO$_2$ and MAP), and PRx index (correlation between ICP and MAP). For the two serial assessments in subject 5, the ORx values were 0.80 ($p < 0.0001$) and 0.69 ($p < 0.0001$); the COx values were 0.72 ($p < 0.0001$) and 0.19 ($p = 0.01$), and the PRx values were 0.10 ($p = 0.34$) and 0.92 ($p < 0.0001$). TDF data were not available during these CA assessments.

Across all of the MAP challenges, indices using CBF or CBF proxies (i.e. PbtO$_2$, StO$_2$) showed overall impaired CA (Figure 5(a),(b)). The median (25th percentile, 75th percentile) DCSx index across the MAP challenges was 0.69 (0.51, 0.79). Similarly, the median ORx, TDFx, and COx indices were 0.84 (0.67, 0.90), 0.63 (0.28, 0.74), and 0.53 (0.21, 0.73), respectively. In contrast, the median PRx index of 0.12 (0.45, 0.61) was lower, and PRx was frequently discordant with DCSx (Figure 5(c)). The Pearson's correlations between DCSx and ORx ($R = 0.35$, $p = 0.2$), DCSx and TDFx ($R = -0.04$, $p = 0.9$), DCSx and COx ($R = 0.32$, $p = 0.2$), and DCSx and PRx ($R = 0.18$, $p = 0.5$) were all not significant (Fisher transformation applied to CA indices prior to computing Pearson's correlations[60]).

Steady-state changes in CBF (measured by both NNOM and invasive TDF), OEF (measured by NNOM), and PbtO$_2$ were also calculated between 6-min averages (mean) of temporally stable data acquired shortly after (e.g., vertical dashed lines in Figure 4(a),(b)) and shortly before (e.g., solid red lines in Figure 4(a),(b)) medication rate adjustments. The steady-state NNOM CBF changes were strongly correlated with PbtO$_2$ changes ($R = 0.82$, $p = 0.0002$; Figure 5(d)), which is consistent with prior work.[20] However, NNOM CBF changes were not significantly correlated with invasive TDF CBF changes ($R = 0.49$,
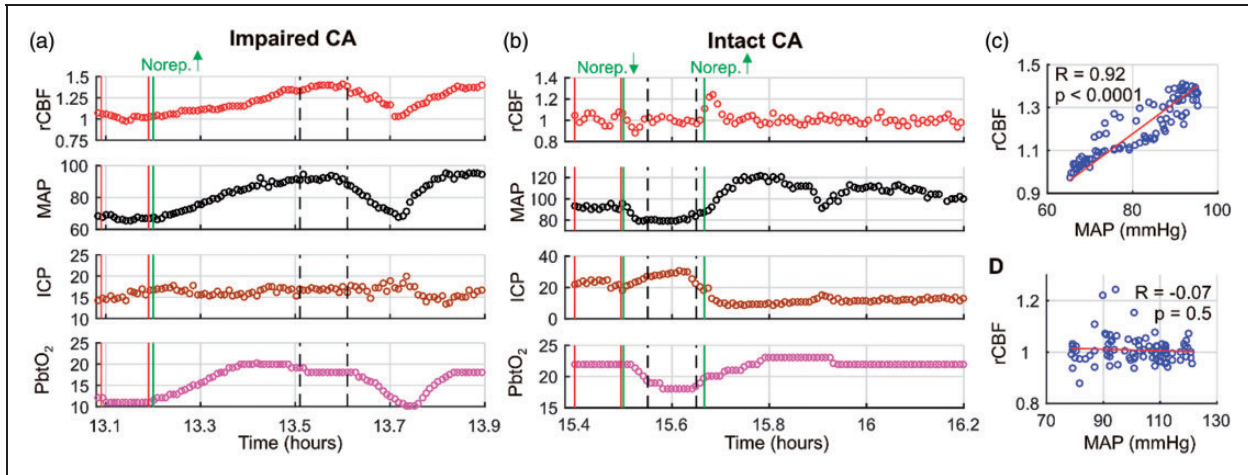
Figure 4. Temporal non-invasive neurometabolic optical monitor (NNOM) measurements of relative cerebral blood flow (rCBF   CBF/CBF$_o$) with concurrent mean arterial pressure (MAP, mmHg), intracranial pressure (ICP, mmHg), and brain interstitial oxygen tension (PbtO$_2$, mmHg) data acquired during MAP manipulations performed on "measurement day 1" (a) and "measurement day 2" (b) in subject #5 (diagnosed with traumatic brain injury, see Table 1). CBF$_o$ is the (baseline) mean value of the data between the two vertical red lines. MAP was significantly altered via adjustment of norepinephrine infusion (vertical green lines: the increase from 2 to 4 mcg/kg/min in panel (a); the decrease from 4 to 2 mcg/kg/min, followed by the increase from 2 to 4 mcg/kg/min in panel (b)). The vertical dashed black lines indicate the 6-min intervals used to compute the steady-state changes relative to baseline that are shown in panels (d) and (e) of Figure 5. (c) rCBF plotted against concurrent MAP data for the entire temporal interval shown in panel (a). The high Pearson's correlation coefficient (i.e., DCSx = 0.92, $p < 0.0001$) indicates impaired cerebral autoregulation (CA). (d) rCBF plotted against concurrent MAP data for the entire temporal interval shown in panel (b). The lack of correlation (i.e., DCSx = − 0.07, $p = 0.5$) indicates intact CA. The analogous pressure reactivity autoregulation indices (PRx) for the data in panels (a) and (b) are   0.10 ($p = 0.34$) and   0.92 ($p < 0.0001$), respectively (note, although the PRx value for panel (a) is negative, the p value indicates the correlation is not significant). The analogous brain tissue oxygen pressure reactivity autoregulation indices (ORx) are 0.80 ($p < 0.0001$) and 0.69 ($p < 0.0001$), respectively. Thermal diffusion flowmetry data were not available during these CA assessments.

$p = 0.2$; Figure 5(f)). In regards to brain oxygenation, steady-state changes in OEF measured with NNOM during the MAP challenges were not significantly correlated with PbtO$_2$ changes ($R = −$ 0.23, $p = 0.4$; Figure 5(e)), which is also consistent with prior work.[20]

Changes in CBF triggered by vasoactive medications were often, but not always, associated with perfusion-metabolism mismatches as well. OEF and CMRO$_2$ increased significantly in five of the 12 cases in Figure 5 where NNOM CBF decreased; these observations suggest that ischemia is triggered by cerebral hypoperfusion. OEF and CMRO$_2$ similarly increased for two of the remaining seven episodes where NNOM CBF increased; these observations suggest that relative ischemia arises from cerebral hypermetabolism. These CMRO$_2$ increases are associated with increasing norepinephrine infusion rates and may be indicative of drug-mediated neuroactivation facilitated by a disrupted BBB.[61]

Discussion

In this study, we demonstrate the clinical promise of continuously and concurrently measuring changes in CBF, StO$_2$, and CMRO$_2$ in critically ill brain injured patients by combining DCS with TR-NIRS into a

single NNOM. Along with combining DCS and TR-NIRS, we utilized a two-layer head model to filter superficial tissue contamination in relative StO$_2$ and CBF data. NNOM enabled combined measurements of CA (e.g., Figures 4 and 5) with the unambiguous identification of mismatches between cerebral perfusion and metabolism (e.g., Figures 2 and 3). NNOM further uniquely revealed the type of processes triggering the mismatch (e.g., low oxygen delivery, high oxygen demand), which is relevant for optimal clinical decision-making. Importantly, the identified episodes of metabolism/perfusion mismatch were not detected by any of the other methods of monitoring used clinically in our patient cohort.

Identification of cerebral perfusion/metabolism mismatches

Prevention of delayed secondary brain injury, which is caused in large part by mismatches between CBF and metabolic demand, remains a fundamental goal of neurocritical care. Metabolism/perfusion mismatches occur both when demand exceeds perfusion (ischemia) and when perfusion exceeds demand (hyperemia), and these effects are magnified by impairments in CA and
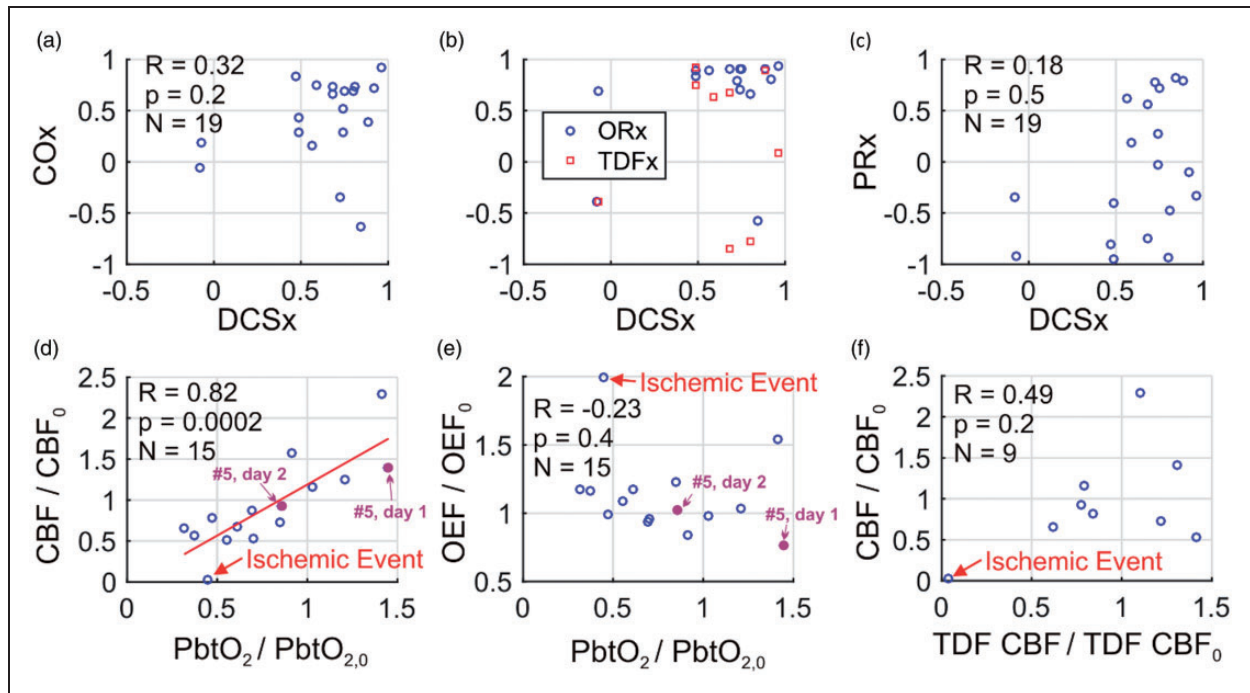
Figure 5. During non-invasive neurometabolic optical monitoring, significant mean arterial pressure (MAP) changes were induced 19 times by standard-of-care adjustment in vasoactive medication infusion rates. DCSx, COx, ORx, TDFx, and PRx cerebral autoregulation (CA) indices were computed across the 50-min intervals encompassing the infusion changes (see text). These five indices are, respectively, the Pearson correlation coefficients between: (1) optical diffuse correlation spectroscopy (DCS) cerebral blood flow (CBF) index and mean arterial pressure (MAP); (2) optical time-resolved near-infrared spectroscopy (TR-NIRS) measurement of cerebral tissue oxygen saturation and MAP; (3) brain interstitial oxygen tension ($PbtO_2$) and cerebral perfusion pressure (CPP); (4) thermal diffusion flowmetry (TDF) CBF and CPP; and (5) MAP and intracranial pressure. (a) COx plotted against DCSx; (b) ORx (blue circles) and TDFx (red squares) plotted against DCSx; and (c) PRx plotted against DCSx. In most cases, the DCSx, COx, ORx, and TDFx indicate impaired CA. The PRx, however, is more variable. Steady-state $PbtO_2$ changes resulting from the infusion changes were correlated with DCS measured CBF changes (equation (3)) (d), but not with TR-NIRS measured OEF changes (equation (2)) (e). Steady-state DCS measured CBF changes were not correlated with TDF CBF changes (f). In panels (d) through (f), the baseline and perturbed data are 6 min averages across stable data acquired shortly before and shortly after the pressor infusion rate changes (e.g., see Figure 4). The red line in panel (d) is the linear best-fit line. One event of cerebral ischemia (i.e., $PbtO_2 < 20$ mmHg, TDF CBF < 15 ml/100 g/min, cerebral microdialysis lactate:pyruvate ratio > 40) accompanied a drop in phenylephrine infusion (labeled in panels (d), (e), (f); temporal data in Figure 2). For subject #5, DCSx indicated impaired CA day 1 (DCSx $= 0.92$), and intact CA day 2 (DCSx $= -0.07$; MAP challenges labeled in panels (d), (e); temporal data in Figure 4).

neurovascular coupling that occur as a consequence of the initial insult. The deleterious consequences of both ischemia and hyperemia are underscored by population-based studies showing that mortality increases when blood pressure is maintained below the autoregulatory limit, while rates of severe disability and clinically significant hemorrhage increase if blood pressure exceeds the limits of autoregulation.[62–64]

Individualized titration of cerebral perfusion to the metabolic needs of the injured brain could therefore markedly improve outcome after brain injury. The complementary information provided by NNOM reduces ambiguities that arise from isolated CBF and cerebral oxygenation measurements alone.[33,35] For example, low StO_2 measured by commercial NIRS oximeters could correspond to abnormally low oxygen delivery (e.g., ischemia) or abnormally high

oxygen demand (e.g., seizure). In addition, a tissue volume with normal StO_2 could be healthy, or it could also reflect decreased metabolic activity arising from impaired oxygen delivery or pathologic changes in the venous admixture. Changes in CBF can be similarly confounded by sedation (such that CBF is reduced to compensate for decreased metabolic activity) or high metabolic demand (where increased CBF may not match increases in cerebral metabolism).

By measuring CBF and StO_2 simultaneously, we successfully distinguished between ischemic conditions that arose from decreases in oxygen delivery and from increases in oxygen demand (Figure 2). We further detected potentially deleterious hyperemia that occurred in the setting of a rapid reduction in ICP (Figure 3). Importantly, these conditions would not have been identified without the combined information

about CBF and StO_2 provided by the NNOM. Although invasive neuromonitoring did identify physiological distress during these episodes (e.g., reduced $PbtO_2$, increasing LPR), the invasive data were unable to categorize the type of process that triggered these abnormalities. Obtaining such information will be crucial to inform appropriate treatment choices, and we envision the NNOM will become a useful clinical tool in neurocritical care for rapid, non-invasive identification of ischemia.

We note that the two-layer head model utilized herein was important for quantitative accuracy of the magnitude of the NNOM changes. The NNOM trends derived from applying the homogeneous semi-infinite model to the long separation data were consistent with the two-layer results, but the magnitudes of the changes were substantially different (see Supplementary material).

Utility of relative NNOM data

Our observations are based on relative changes in NNOM parameters, which can be valuable for detecting abrupt changes in patient status. We noted several situations in Table S1 of the Supplementary material wherein relative NNOM data may be clinically helpful. Moreover, current research suggests that a single indocyanine green (ICG) bolus injection may enable calibration of the NNOM system and thereafter facilitate continuous monitoring of absolute CBF and $CMRO_2$.[45,65,66]

Non-invasive CA measurements

We also measured CA by calculating the correlation between changes in CBF and MAP. Measurement of cerebral autoregulatory state may help clinicians titrate hemodynamic targets after brain injury (so that blood pressures are kept in a range where CA is optimally preserved[67]), and also may aid in neuro-prognostication (since the degree of autoregulation failure is a robust predictor of outcome after severe brain injury).[10,55,68–70] In our study, we assessed autoregulation during episodes where blood pressure changed in the setting of vasoactive medication dosage titrations. The ability to continuously measure changes in CBF should also allow longitudinal assessments of CA changes over time by computing correlations between CBF and spontaneous blood pressure fluctuations. Similar continuously updated indices of autoregulation have been constructed by measuring correlations between ICP, $PbtO_2$, StO_2, and TCD based measurements of flow velocity,[10,55,57,68–70] and a very recent paper demonstrated the potential utility of DCS to continuously measure CA in the ICU.[36]

Our results are consistent with this latter paper's findings of impaired CA in most patients (Figure 5). In an interesting case example, we further used DCS to show longitudinal improvement in CA (Figure 4) in a patient who ultimately recovered consciousness. Since DCS directly measures CBF, the DCSx index has potential to be a more sensitive and accurate non-invasive assessment of CA than other proposed CA assessments relying on CBF proxies (e.g., $PbtO_2$, StO_2, TCD). In aggregate, the conclusions about CA assessed by DCSx, ORx, COx, and TDFx were consistent (Figure 5), but substantial variability between the DCSx index and other indices of CA across subjects was observed (Figure 5). We also observed discrepancies between CBF-based CA indices and the PRx. Future work is needed to more fully compare these indices, and relate them to neurological outcome.

Agreement with invasive absolute CBF and oxygenation measurements

Across all patient data wherein TDF/DCS and $PbtO_2$/StO_2/DCS results were concurrently obtained, our non-invasive absolute CBF and StO_2 measurements correlated poorly with absolute invasive CBF and brain oxygenation measures, respectively. While initially surprising, multiple explanations for this finding are readily evident.

First, because invasive and non-invasive CBF measurements interrogate different vascular beds (white matter for invasive TDF, and cortex for DCS), fluctuations in blood flow measured by these two probes need not closely track one another. In a similar vein, the spatiotemporal patterns of CBF can vary markedly across hemispheres; this issue is especially relevant for the subgroup of patients for whom it was necessary to place the NNOM probe on the hemisphere opposite to that of the bolt (see Table 2).

Second, TDF measurements have been reported to drift significantly over time, requiring frequent recalibration.[18,19] This pronounced drift, which we also observed in the present investigation, can significantly degrade the overall correlation between TDF CBF and other measurements of CBF.

Third, in general the DCS measurements are sensitive to confounding factors such as scalp blood flow contamination, errors in tissue optical property measurements, motion artifacts, and changes in scalp/skull thickness due to differences in probe pressure and probe location that arise during prolonged monitoring.[36,45,51,71,72] We ameliorated the first confounder by using a two-layer head model to filter extra-cerebral artifacts, but our analysis is still sensitive to the other confounders that need to be addressed in future work. For example, to reduce cross talk between unknown

fitting parameters, the present analysis assumed constant tissue scattering to compute differential changes. Although this assumption is often reasonable,[73] it can lead to errors if tissue structure substantially changes (e.g., edema). For the case examples reported in this work, however, the temporal variations of tissue reduced scattering, obtained by fitting TR-NIRS measurements with the long-separation source-detector data with the homogeneous semi-infinite tissue model, were less than 5%. Another confounder is heterogeneous tissue optical properties. The present analysis uses tissue optical properties obtained from nonlinear fit of the baseline TR-NIRS signal to the semi-infinite homogeneous solution of the photon diffusion equation in order to estimate cerebral and extra-cerebral tissue sensitivity factors (see Supplementary material). Errors in these estimated sensitivity factors that arise from heterogeneous tissue optical properties will translate to smaller errors in hemodynamic changes that do not change the conclusions of the case examples (see Supplementary material).[73]

Finally, because $PbtO_2$ measurements exhibit a complex dependence on both cerebral perfusion and the arteriovenous gradient in free oxygen tension,[20,74] both CBF and StO_2 measurements would be expected to correlate poorly with $PbtO_2$ over long measurement periods. Indeed, prior work from our group and from others show weak, if any, correlation between brain oxygen saturation and $PbtO_2$ measurements.[37,75,76]

Despite the poor correlations between absolute non-invasive and invasive measurements over long time scales, we nevertheless demonstrated the ability of NNOM to provide physiologically meaningful data during blood pressure manipulations and other clinical events that were concordant with invasive monitoring. These data provide pilot validation of NNOM's ability to detect ischemic conditions and ischemic risk factors (i.e., impaired CA), and further builds upon our initial analysis suggesting that DCS CBF measurements can detect brain hypoxia identified by $PbtO_2$.[37] Moreover, some of our observations suggest that decisions based on systemic variables alone may produce deleterious intracranial results (e.g., blood pressure lowering example in Figure 2(a)).

Prolonged monitoring in the ICU

Physiological monitoring in the intensive care unit (ICU) presents unique challenges due to the presence of numerous other monitors that can interfere with measurement fidelity, as well as artifacts caused by patient agitation, nursing care, bedside procedures, and transport to and from other diagnostic/imaging studies. As demonstrated by our group and others,[36,38,45,77,78,79–87] diffuse optics is well-suited for continuous, long-term monitoring of

patients. Accordingly, we were able to perform continuous stretches of optical monitoring for several hours/day in all our patients. The length of these monitoring sessions was not limited by technical issues, but rather only by the need to have research staff present. Thus, we foresee straightforward translation to monitoring that can be performed continuously for days.

Limitations and future directions

Our study has several limitations. Because of the small sample number and study design, we were constrained in our analysis to retrospectively focus on specific episodes of clinical interest that were marked for further review during the monitoring sessions. Future work investigating pre-specified outcome-measures in larger cohorts with specific types of brain injury (e.g., accurate detection of delayed cerebral ischemia after aneurysm rupture, or detection of hyperemic states after endovascular thrombectomy for ischemic stroke) will be required before translation to routine clinical use. Nevertheless, we identified clear instances of impaired autoregulation and perfusion/metabolism failure that have immediate clinical implications. Moreover, we have recently reported the capability of NNOM DCS monitoring to detect brain hypoxia based on $PbtO_2$.[37]

The poor overall correlation between our absolute optical and invasive CBF and oxygenation measures may be due in to the challenges of absolute CBF monitoring with DCS. Although assessment of relative changes in cerebrovascular physiology with diffuse optics is robust, reliable absolute CBF measurements with DCS are needed for comparisons of optical CBF and $CMRO_2$ indices across multiple patients, between hemispheres in a single patient, and across multiple monitoring sessions. A potential solution is to calibrate DCS with an absolute CBF measurement obtained from a dynamic contrast enhanced NIRS approach that tracks the passage of an intravenously injected NIR absorbable dye (indocyanine green) through cerebral tissue.[45,65,66,72,79] Combining this approach with TR-NIRS-based oxygen saturation measurements may allow continuous non-invasive absolute $CMRO_2$ measurements in the future. Further work will be required, however, to validate these methods with existing gold standards such as positron emission tomography. Once validated, absolute thresholds for both ischemia (defined by excess $CMRO_2$ relative to CBF) and hyperemia (defined by excess CBF relative to $CMRO_2$) can be defined for clinical use.

Conclusion

We utilized simultaneous, continuous optical measurements of CBF and $CMRO_2$ changes to non-invasively

detect deleterious mismatches between cerebral perfusion and oxygen metabolism (3 events) that spontaneously arose in patients with severe acute brain injury. These mismatches were concordant with physiological distress indicated by invasive neuromonitoring. In addition, the optical CBF and $CMRO_2$ data, in combination, uniquely revealed the type of process triggering the mismatch (e.g., abnormally low oxygen delivery, abnormally high oxygen demand). Less severe mismatches between perfusion and metabolism were further detected in events (6 events) associated with vasoactive medication changes. Finally, we demonstrated the ability to perform non-invasive, longitudinal assessments of CA (19 events) based on optical CBF measurements.

ORCID iD

Wesley B Baker (ID) https://orcid.org/0000-0002-3025-6061
Elizabeth Mahanna Gabrielli (ID) https://orcid.org/0000-0002-1297-1432

Supplemental Material

Supplemental material for this article is available online.

References

1. Al-Tamimi YZ, Orsi NM, Quinn AC, et al. A review of delayed ischemic neurologic deficit following aneurysmal subarachnoid hemorrhage: historical overview, current treatment, and pathophysiology. *World Neurosurg* 2010; 73: 654–667.
2. Cunningham A, Salvador R, Coles J, et al. Physiological thresholds for irreversible tissue damage in contusional regions following traumatic brain injury. *Brain* 2005; 128: 1931–1942.
3. Vergouwen MD, Vermeulen M, van Gijn J, et al. Definition of delayed cerebral ischemia after aneurysmal subarachnoid hemorrhage as an outcome event in clinical trials and observational studies. *Stroke* 2010; 41: 2391–2395.
4. Werner C and Engelhard K. Pathophysiology of traumatic brain injury. *Br J Anaesth* 2007; 99: 4–9.
5. Brott T and Bogousslavsky J. Treatment of acute ischemic stroke. *N Engl J Med* 2000; 343: 710–722.
6. Le Roux P. Physiological monitoring of the severe traumatic brain injury patient in the intensive care unit. *Curr Neurol Neurosci Rep* 2013; 13: 1–16.
7. Sandsmark DK, Kumar MA, Park S, et al. Multimodal monitoring in subarachnoid hemorrhage. *Stroke* 2012; 43: 1440–1445.
8. Oddo M, Villa F and Citerio G. Brain multimodality monitoring: an update. *Curr Opin Crit Care* 2012; 18: 111–118.
9. Roh D and Park S. Brain multimodality monitoring: updated perspectives. *Curr Neurol Neurosci Rep* 2016; 16: 56.
10. Budohoski KP, Czosnyka M, Smielewski P, et al. Impairment of cerebral autoregulation predicts delayed cerebral ischemia after subarachnoid hemorrhage: a prospective observational study. *Stroke* 2012; 43: 3230–3237.
11. Sinha S, Hudgins E, Schuster J, et al. Unraveling the complexities of invasive multimodality neuromonitoring. *Neurosurg Focus* 2017; 43: E4.
12. Rosner MJ, Rosner SD and Johnson AH. Cerebral perfusion pressure: management protocol and clinical results. *J Neurosurg* 1995; 83: 949–962.
13. Schmidt JM, Ko S-B, Helbok R, et al. Cerebral perfusion pressure thresholds for brain tissue hypoxia and

metabolic crisis after poor-grade subarachnoid hemorrhage. *Stroke* 2011; 42: 1351–1356.

14. Kato R and Pinsky MR. Personalizing blood pressure management in septic shock. *Ann Intensive Care* 2015; 5: 1.

15. Okonkwo DO, Shutter LA, Moore C, et al. Brain oxygen optimization in severe traumatic brain injury phase-II: a phase II randomized trial. *Crit Care Med* 2017; 45: 1907–1914.

16. Stein NR, McArthur DL, Etchepare M, et al. Early cerebral metabolic crisis after TBI influences outcome despite adequate hemodynamic resuscitation. *Neurocrit Care* 2012; 17: 49–57.

17. Vespa PM, O'Phelan K, McArthur D, et al. Pericontusional brain tissue exhibits persistent elevation of lactate/pyruvate ratio independent of cerebral perfusion pressure. *Crit Care Med* 2007; 35: 1153–1160.

18. Jaeger M, Soehle M, Schuhmann MU, et al. Correlation of continuously monitored regional cerebral blood flow and brain tissue oxygen. *Acta Neurochir* 2005; 147: 51–56; discussion 6.

19. Wolf S, Vajkoczy P, Dengler J, et al. Drift of the Bowman Hemedex(R) cerebral blood flow monitor between calibration cycles. *Acta Neurochir Suppl* 2012; 114: 187–190.

20. Rosenthal G, Hemphill JC 3rd, Sorani M, et al. Brain tissue oxygen tension is more indicative of oxygen diffusion than oxygen delivery and metabolism in patients with traumatic brain injury. *Crit Care Med* 2008; 36: 1917–1924.

21. Sahuquillo J, Amoros S, Santos A, et al. Does an increase in cerebral perfusion pressure always mean a better oxygenated brain? A study in head-injured patients. *Acta Neurochir Suppl* 2000; 76: 457–462.

22. Larach DB, Kofke WA and Le Roux P. Potential non-hypoxic/ischemic causes of increased cerebral interstitial fluid lactate/pyruvate ratio: a review of available literature. *Neurocrit Care* 2011; 15: 609–622.

23. Magistretti PJ and Allaman I. Lactate in the brain: from metabolic end-product to signalling molecule. *Nat Rev Neurosci* 2018; 19: 235–249.

24. Oddo M, Levine JM, Frangos S, et al. Brain lactate metabolism in humans with subarachnoid hemorrhage. *Stroke* 2012; 43: 1418–1421.

25. Foreman B and Claassen J. Quantitative EEG for the detection of brain ischemia. *Crit Care* 2012; 16: 216.

26. Sharbrough FW, Messick JM Jr and Sundt TM Jr. Correlation of continuous electroencephalograms with cerebral blood flow measurements during carotid endarterectomy. *Stroke* 1973; 4: 674–683.

27. Bishop CC, Powell S, Rutt D, et al. Transcranial Doppler measurement of middle cerebral artery blood flow velocity: a validation study. *Stroke* 1986; 17: 913–915.

28. Torricelli A, Contini D, Pifferi A, et al. Time domain functional NIRS imaging for human brain mapping. *Neuroimage* 2014; 85: 28–50.

29. Pifferi A, Contini D, Dalla Mora A, et al. New frontiers in time-domain diffuse optics, a review. *J Biomed Opt* 2016; 21: 091310.

30. Durduran T and Yodh AG. Diffuse correlation spectroscopy for non-invasive, micro-vascular cerebral blood flow measurement. *NeuroImage* 2014; 85: 51–63.

31. Shang Y, Li T and Yu G. Clinical applications of near-infrared diffuse correlation spectroscopy and tomography for tissue blood flow monitoring and imaging. *Physiol Meas* 2017; 38: R1.

32. Buckley EM, Parthasarathy AB, Grant EP, et al. Diffuse correlation spectroscopy for measurement of cerebral blood flow: future prospects. *Neurophotonics* 2014; 1: 011009.

33. Culver JP, Durduran T, Furuya D, et al. Diffuse optical tomography of cerebral blood flow, oxygenation, and metabolism in rat during focal ischemia. *J Cereb Blood Flow Metab* 2003; 23: 911–924.

34. Verdecchia K, Diop M, Lee T-Y, et al. Quantifying the cerebral metabolic rate of oxygen by combining diffuse correlation spectroscopy and time-resolved near-infrared spectroscopy. *J Biomed Opt* 2013; 18: 027007.

35. Boas DA and Franceschini MA. Haemoglobin oxygen saturation as a biomarker: the problem and a solution. *Philos Trans Ser A Math Phys Eng Sci* 2011; 369: 4407–4424.

36. Selb J, Wu K-C, Sutin J, et al. Prolonged monitoring of cerebral blood flow and autoregulation with diffuse correlation spectroscopy in neurocritical care patients. *Neurophotonics* 2018; 5: 045005.

37. Busch DR, Balu R, Baker WB, et al. Detection of brain hypoxia based on noninvasive optical monitoring of cerebral blood flow with diffuse correlation spectroscopy. *Neurocrit Care* 2019; 30: 72–80.

38. Davies DJ, Clancy M, Dehghani H, et al. Cerebral oxygenation in traumatic brain injury: can a non-invasive frequency domain near-infrared spectroscopy device detect changes in brain tissue oxygen tension as well as the established invasive monitor? *J Neurotrauma* 2019; 36: 1175–1183.

39. Frontera J, Ziai W, O'Phelan K, et al. Regional brain monitoring in the neurocritical care unit. *Neurocrit Care* 2015; 22: 348–359.

40. Smith M. Cerebral microdialysis. In: Le Roux P, Levine JM and Kofke WA (eds) *Monitoring in neurocritical care*. 1st ed. Philadelphia, PA: Elsevier Saunders, 2013.

41. Bellander B-M, Cantais E, Enblad P, et al. Consensus meeting on microdialysis in neurointensive care. *Intensive Care Med* 2004; 30: 2166–2169.

42. Reinstrup P, Ståhl N, Mellergård P, et al. Intracerebral microdialysis in clinical practice: baseline values for chemical markers during wakefulness, anesthesia, and neurosurgery. *Neurosurgery* 2000; 47: 701–710.

43. Marshall LF, Marshall SB, Klauber MR, et al. The diagnosis of head injury requires a classification based on computed axial tomography. *J Neurotrauma* 1992; 9: S287–S292.

44. Hemphill JC 3rd, Bonovich DC, Besmertis L, et al. The ICH score: a simple, reliable grading scale for intracerebral hemorrhage. *Stroke* 2001; 32: 891–897.

45. He L, Baker WB, Milej D, et al. Noninvasive continuous optical monitoring of absolute cerebral blood flow in critically ill adults. *Neurophotonics* 2018; 5: 045006.

46. Liebert A, Wabnitz H and Elster C. Determination of absorption changes from moments of distributions of times of flight of photons: optimization of measurement conditions for a two-layered tissue model. *J Biomed Opt* 2012; 17: 057005.

47. Liebert A, Wabnitz H, Steinbrink J, et al. Time-resolved multidistance near-infrared spectroscopy of the adult head: intracerebral and extracerebral absorption changes from moments of distribution of times of flight of photons. *Appl Opt* 2004; 43: 3037–3047.

48. Durduran T, Choe R, Baker WB, et al. Diffuse optics for tissue monitoring and tomography. *Rep Prog Phys* 2010; 73: 076701.

49. Selb J, Joseph DK and Boas DA. Time-gated optical system for depth-resolved functional brain imaging. *J Biomed Opt* 2006; 11: 044008.

50. Kienle A and Patterson MS. Improved solutions of the steady-state and the time-resolved diffusion equations for reflectance from a semi-infinite turbid medium. *J Opt Soc Am A Opt Image Sci Vision* 1997; 14: 246–254.

51. Baker WB, Parthasarathy AB, Ko TS, et al. Pressure modulation algorithm to separate cerebral hemodynamic signals from extracerebral artifacts. *Neurophotonics* 2015; 2: 035004.

52. Mesquita RC, Durduran T, Yu G, et al. Direct measurement of tissue blood flow and metabolism with diffuse optics. *Philos Trans Ser A Math Phys Eng Sci* 2011; 369: 4390–4406.

53. Jain V, Buckley EM, Licht DJ, et al. Cerebral oxygen metabolism in neonates with congenital heart disease quantified by MRI and optics. *J Cereb Blood Flow Metab* 2014; 34: 380–388.

54. Valabregue R, Aubert A, Burger J, et al. Relation between cerebral blood flow and metabolism explained by a model of oxygen exchange. *J Cereb Blood Flow Metab* 2003; 23: 536–545.

55. Czosnyka M, Smielewski P, Kirkpatrick P, et al. Continuous assessment of the cerebral vasomotor reactivity in head injury. *Neurosurgery* 1997; 41: 11–19.

56. Jaeger M, Schuhmann MU, Soehle M, et al. Continuous assessment of cerebrovascular autoregulation after traumatic brain injury using brain tissue oxygen pressure reactivity. *Crit Care Med* 2006; 34: 1783–1788.

57. Brady KM, Lee JK, Kibler KK, et al. Continuous time-domain analysis of cerebrovascular autoregulation using near-infrared spectroscopy. *Stroke* 2007; 38: 2818–2825.

58. Schulz MK, Wang LP, Tange M, et al. Cerebral microdialysis monitoring: determination of normal and ischemic cerebral metabolisms in patients with aneurysmal subarachnoid hemorrhage. *J Neurosurg* 2000; 93: 808–814.

59. Ståhl N, Mellergård P, Hallstrom A, et al. Intracerebral microdialysis and bedside biochemical analysis in patients with fatal traumatic brain lesions. *Acta Anaesthesiol Scand* 2001; 45: 977–985.

60. Silver NC and Dunlap WP. Averaging correlation coefficients: should Fisher's z transformation be used? *J Appl Psychol* 1987; 72: 146.

61. MacKenzie E, McCulloch J, O'kean M, et al. Cerebral circulation and norepinephrine: relevance of the blood–brain barrier. *Am J Physiol Legacy Content* 1976; 231: 483–488.

62. Mistry EA, Mistry AM, Nakawah MO, et al. Systolic blood pressure within 24 hours after thrombectomy for acute ischemic stroke correlates with outcome. *J Am Heart Assoc* 2017; 6: e006167.

63. Aries MJ, Czosnyka M, Budohoski KP, et al. Continuous determination of optimal cerebral perfusion pressure in traumatic brain injury. *Crit Care Med* 2012; 40: 2456–2463.

64. Martins AI, Sargento-Freitas J, Silva F, et al. Recanalization modulates association between blood pressure and functional outcome in acute ischemic stroke. *Stroke* 2016; 47: 1571–1576.

65. Milej DF, He L, Abdalmalak A, et al. Quantification of cerebral blood flow in adults by dynamic contrast-enhanced NIRS: validation against MRI. Optics and the Brain. *Optical Society of America* 2018; Optics and Brain: p.BF2C.

66. Elliott JT, Diop M, Morrison LB, et al. Quantifying cerebral blood flow in an adult pig ischemia model by a depth-resolved dynamic contrast-enhanced optical method. *NeuroImage* 2014; 94: 303–311.

67. Steiner LA, Czosnyka M, Piechnik SK, et al. Continuous monitoring of cerebrovascular pressure reactivity allows determination of optimal cerebral perfusion pressure in patients with traumatic brain injury. *Crit Care Med* 2002; 30: 733–738.

68. Czosnyka M, Brady K, Reinhard M, et al. Monitoring of cerebrovascular autoregulation: facts, myths, and missing links. *Neurocrit Care* 2009; 10: 373–386.

69. Jaeger M, Schuhmann MU, Soehle M, et al. Continuous monitoring of cerebrovascular autoregulation after subarachnoid hemorrhage by brain tissue oxygen pressure reactivity and its relation to delayed cerebral infarction. *Stroke* 2007; 38: 981–986.

70. Budohoski KP, Reinhard M, Aries MJ, et al. Monitoring cerebral autoregulation after head injury. Which component of transcranial Doppler flow velocity is optimal? *Neurocrit Care* 2012; 17: 211–218.

71. Mesquita RC, Schenkel SS, Minkoff DL, et al. Influence of probe pressure on the diffuse correlation spectroscopy blood flow signal: extra-cerebral contributions. *Biomed Opt Express* 2013; 4: 978–994.

72. Diop M, Verdecchia K, Lee T-Y, et al. Calibration of diffuse correlation spectroscopy with a time-resolved near-infrared technique to yield absolute cerebral blood flow measurements. *Biomed Opt Express* 2011; 2: 2068–2081.

73. Baker WB, Parthasarathy AB, Busch DR, et al. Modified Beer–Lambert law for blood flow. *Biomed Opt Express* 2014; 5: 4053–4075.

74. Dings J, Meixensberger J, Jager A, et al. Clinical experience with 118 brain tissue oxygen partial pressure catheter probes. *Neurosurgery* 1998; 43: 1082–1094.

75. Leal-Noval SR, Cayuela A, Arellano-Orden V, et al. Invasive and noninvasive assessment of cerebral oxygenation in patients with severe traumatic brain injury. *Intensive Care Med* 2010; 36: 1309–1317.

76. Kerz T, Beyer C, Huthmann A, et al. Continuous-wave near-infrared spectroscopy is not related to brain tissue oxygen tension. *J Clin Monit Comput* 2016; 30: 641–647.

77. Zirak P, Gregori-Pla C, Blanco I, et al. Characterization of the microvascular cerebral blood flow response to obstructive apneic events during night sleep. *Neurophotonics* 2018; 5: 045003.

78. Busch DR, Rusin CG, Miller-Hance W, et al. Continuous cerebral hemodynamic measurement during deep hypothermic circulatory arrest. *Biomed Opt Express* 2016; 7: 3461–3470.

79. Diop M, Kishimoto J, Toronov V, et al. Development of a combined broadband near-infrared and diffusion correlation system for monitoring cerebral blood flow and oxidative metabolism in preterm infants. *Biomed Opt Express* 2015; 6: 3907–3918.

80. Nourhashemi M, Kongolo G, Mahmoudzadeh M, et al. Relationship between relative cerebral blood flow, relative cerebral blood volume, and relative cerebral metabolic rate of oxygen in the preterm neonatal brain. *Neurophotonics* 2017; 4: 021104.

81. Lynch JM, Ko T, Busch DR, et al. Preoperative cerebral hemodynamics from birth to surgery in neonates with critical congenital heart disease. *J Thorac Cardiovasc Surg* 2018; 156: 1657–1664.

82. Buckley EM, Lynch JM, Goff DA, et al. Early postoperative changes in cerebral oxygen metabolism following neonatal cardiac surgery: effects of surgical duration. *J Thorac Cardiovasc Surg* 2013; 145: 196–205.e1.

83. Farzam P, Buckley EM, Lin P-Y, et al. Shedding light on the neonatal brain: probing cerebral hemodynamics by diffuse optical spectroscopic methods. *Sci Rep* 2017; 7: 15786.

84. Delgado-Mederos R, Pla C-G, Zirak P, et al. Transcranial diffuse optical assessment of the microvascular reperfusion after thrombolysis for acute ischemic stroke. *Biomed Opt Express* 2018; 9: 1262–1271.

85. Ferradal SL, Yuki K, Vyas R, et al. Non-invasive assessment of cerebral blood flow and oxygen metabolism in neonates during hypothermic cardiopulmonary bypass: feasibility and clinical implications. *Sci Rep* 2017; 7: 44117.

86. Parthasarathy AB, Gannon KP, Baker WB, et al. Dynamic autoregulation of cerebral blood flow measured non-invasively with fast diffuse correlation spectroscopy. *J Cereb Blood Flow Metab* 2018; 38: 230–240.

87. Yucel MA, Selb J, Boas DA, et al. Reducing motion artifacts for long-term clinical NIRS monitoring using collodion-fixed prism-based optical fibers. *Neuroimage* 2014; 85: 192–201.